Potential contour shaping and sheath behavior with wall electrodes and near-wall magnetic fields in Hall thrusters

K. G. Xu, H. Dao, and M. L. R. Walker

Related Articles

Additional information on Phys. Plasmas
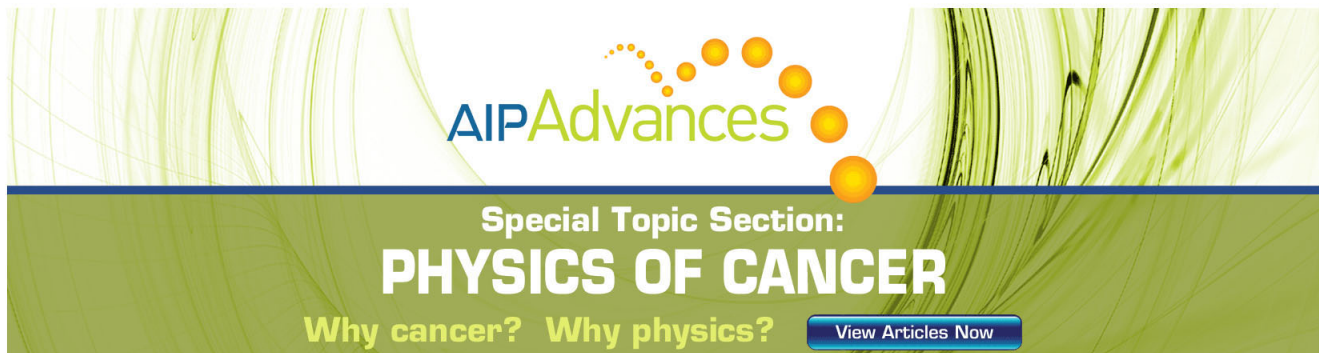
Potential contour shaping and sheath behavior with wall electrodes and near-wall magnetic fields in Hall thrusters

K. G. Xu,[1,a)] H. Dao,[2] and M. L. R. Walker[2]
[1]*Department of Mechanical and Aerospace Engineering, University of Alabama in Huntsville, Huntsville, Alabama 35899, USA*
[2]*Department of Aerospace Engineering, Georgia Institute of Technology, Atlanta, Georgia 30318, USA*

Graphite electrodes are embedded within the discharge channel of a Hall effect thruster to focus ions for improved performance. Cusp-shaped magnetic fields are added around the electrodes to shield the electrodes from high electron current. Internal plasma potential measurements inside the discharge channel show that the presence of floating graphite does not significantly affect the potential contours at 150 V anode potential. Creation of closed contour pockets are observed with the electrodes biased 10 and 30 V above the anode potential. The electrodes also cause a compression of the acceleration region in the thruster. The cause of the changes in the potential contours is attributed to a shifting of discharge electrode from the anode to the electrodes and an expansion of the near-wall plasma sheath. The presence of the cusp magnetic fields is shown to affect the current collected by the electrodes, a behavior associated with modification of the plasma sheath properties due to magnetization of electrons. © 2012 American Institute of Physics. [http://dx.doi.org/10.1063/1.4762856]

I. INTRODUCTION

Hall effect thrusters (HETs) produce thrust through the electrostatic acceleration of ions produced via collisional ionization between propellant neutrals and cathode electrons. Ions are accelerated by the electric field generated between the cathode and the anode to produce thrust. The ion population has a distribution of velocity vectors, some terminating in the discharge channel walls. These ions striking the channel wall are neutralized and leave the thruster without producing significant thrust. Reduction in the loss of ions through wall-neutralization is one method to increase the ion density and performance of HETs. One method to reduce wall collisions is shaping the potential field and, thus, the electric field, within the discharge channel to repel ions. Electric field lines that converge along the channel centerline would both reduce ion wall losses and beam divergence.

In order to control the potential field, secondary electrodes are embedded in the channel wall flush with the surface. The electrodes are biased above anode potential to affect the in-channel plasma potential contours and electric fields. The thruster magnetic field is also designed to produce a magnetic field with high curvature and near-wall cusp fields. The cusp-shaped magnetic fields surround the electrodes to reduce electron current. The magnetic field helps to generate a focused electric field due to the property of thermalized potential, which holds that magnetic field lines approximate equipotential lines. Previous work has shown that biasing the electrodes 10 or 30 V above anode potential increases thrust, specific impulse, thrust-to-power ratio, and anode efficiency.[1] In that work, plume characterization showed decreased plume divergence angle, increase propellant utilization, and increased average ion energy with biased electrodes.

This paper presents in-channel plasma potential measurements of a HET with embedded wall electrodes. Section II presents the embedded electrode, and magnetic field changes made to the HET. Section III discusses the experimental setup including the test facility, the thruster, and the high speed probe system for in-channel potential measurement. Section IV presents the measured potential maps of the in-channel area for the conditions tested. Finally, Sec. V discusses the results and implications.

II. THRUSTER MODIFICATIONS

The HET used in this work is a modified Pratt & Whitney Rocketdyne T-220HT. The original thruster design has a nominal operating power of 10 kW. Thrust data and plume measurements were done by McVey *et al.* at high voltage levels from 300 to 600 V.[2] The modified thruster, named the embedded electrode Hall effect thruster (EEHET), has been tested at the lower voltage range of 125–300 V.[1] The interest in lower voltages is because high thrust-to-power (*T*/P) ratios in HETs tend to peak at lower voltages.[3] Lower voltages also mean lower energy ions, which are strongly affected by changes in the potential field. Two major changes were made to the original T-220HT: replacement of a ring section of boron nitride (BN) wall material with graphite ring electrodes, and redesign of the magnetic field to incorporate cusp fields to shield the electrodes and create a high-curvature concave magnetic field topography. An Electric Propulsion Laboratory 375 series cathode is used as the electron source. The cathode is externally mounted at the 12 o'clock position at 40° from the horizontal. The cathode orifice is located approximately 30 mm axially downstream of the exit plane and 180 mm radially from thruster centerline.

A. Electrodes

The electrodes used in the EEHET are machined from isomolded, super fine grain graphite plates. The pair of rings

---
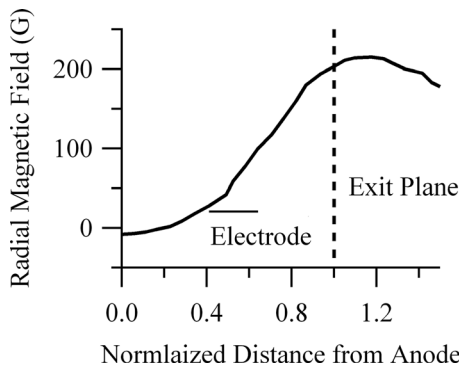
a)Electronic mail: gabe.xu@uah.edu.

FIG. 1. Electrode placement relative to radial magnetic field and channel exit.

is designed to sit within the BN channel wall to preserve a smooth, constant radius channel surface. BN material is removed from the channel to permit addition of the rings. Additional BN rings are used to fill in any space between the electrodes and the channel exit to maintain constant geometry. The location of the electrodes is chosen to be well upstream of the radial magnetic field peak to avoid interference with the region of peak Hall current which has been shown to be near the radial magnetic field peak.[4] Another reason that the electrodes are located so far upstream of the radial peak is to stay away from the ionization/acceleration zones, which has been experimentally found to be correlated to the radial peak,[4,5] and roughly around $0.8 \times B_{r,max}$ where $B_{r,max}$ is the value of the maximum radial magnetic field strength along channel centerline.[6] Fig. 1 shows the radial magnetic field profile for the EEHET and the location of the discharge channel exit plane and electrodes.

Previous work using electrodes in HETs has placed them near the channel exits and, thus, solidly within the ionization/acceleration zones.[7-9] Raitses *et al.* showed the plasma poten-

tial shifts upstream with the presence of floating graphite electrodes.[8] This indicates a shift of the ionization/acceleration region as well. This change was attributed to the lower secondary electron emission (SEE) of graphite compared to BN which increases the electron temperature. It is interesting to note the plasma potential contours became concave with only an inner wall electrode, but with both inner and outer wall electrodes, the contours lost their concavity. In this work, both the inner and outer electrodes are biased together. The single electrode condition was not tested.

The embedded electrodes in this work physically are 10 mm wide and 1.6 mm thick. They are located the same axial distance from the anode, which puts them about 37 mm from the channel exit plane. Fig. 2 shows the electrical schematic for the added electrodes. A discharge filter composed of a RC circuit damps out high frequency oscillations from the main discharge power supply. The key point to note is the electrode power supply is tied to the anode power line, thus the electrode supply only needs to push a few volts to be above anode potential. Even at zero volts on the electrode power supply, the electrodes would be at anode potential if connected.

B. Magnetic field design

The magnetic field topography of the T-220HT is redesigned to include a pair of cusp-shaped fields along the channel wall in order to shield the new electrodes from high electron current. In a standard radial HET magnetic field, the radial field lines would terminate on the electrodes, sinking magnetized electrons into the electrode circuit. By generating cusp fields covering the electrodes, it is hoped electron current can be reduced and any negative impact on the thruster performance due to excess electrode current minimized.

The static magnetic field is simulated with the commercial software MagNet by Infolytica. Fig. 3 shows the final magnetic field topography for the EEHET. The anode and electrodes are labeled. The designed magnetic field has a high concavity for the majority of the channel length. Following the common assumption that magnetic field lines are equipotential contours,[10-12] this will allow an enhanced focusing of the electric field toward centerline. The field also provides ample coverage of the electrodes with cusp fields. The cusp field strength is strong enough to magnetize 25 eV electrons, a conservative estimate for electron temperatures
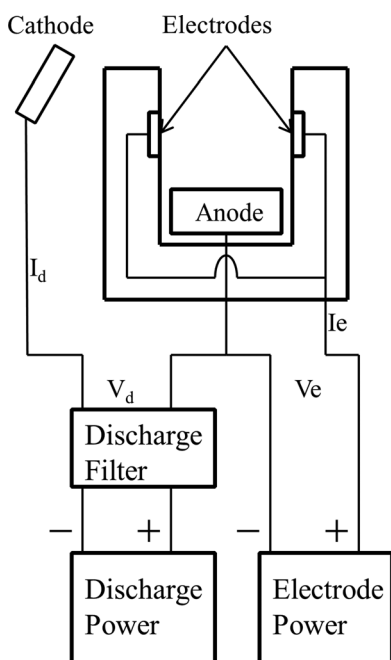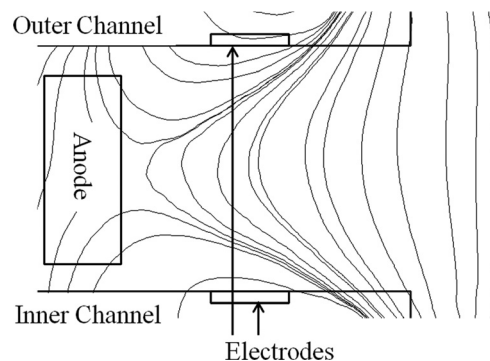

FIG. 2. EEHET electrode wiring diagram.

FIG. 3. Final magnetic field for the EEHET.

near the electrodes based on historical data for HETs of this size.[4,5]

The assumption of magnetic field lines approximating equipotential contours is called the thermalized potential. The thermalized potential is based on the magnetization of electrons by the magnetic field. The electron transport across the magnetic field is small, while the transport along field lines is largely unimpeded. Electrons, being the most energetic charge carriers, determine the local plasma potential. As magnetic fields trap electrons of similar energies, they become potential surfaces. The thermalized potential can be defined as

$$\phi_{th} = \phi_p - \frac{k_B T_e}{e} \ln\left(\frac{n_e}{n_o}\right), \tag{1}$$

where ϕ_p is the plasma potential, k is the Boltzmann constant, T_e is the electron temperature, e is the electron charge, n_e is the electron density, and n_0 is the reference electron density at a reference plasma potential.

The thermalized potential assumption holds when the electron density variation across a field line is low. Due to the high mobility along field lines, the density variations are small. Thus, it can be assumed that the thermalized potential is constant along a magnetic field line. The magnetic field lines are equipotentials within kT_e/e order of accuracy. The low density variation and thermalized potential occur when the electron temperature is low and uniform along a field line. In HETs, this is generally only true in the near anode or plume regions. Near the exit where the Hall current is high and the electron temperature is high, the equipotential lines deviate from the magnetic field lines. Nonetheless, this relation between magnetic field lines and equipotentials helps the magnetic field to alter ion trajectories as electric fields are perpendicular to equipotentials.

III. EXPERIMENTAL SETUP

The experiment is carried out in vacuum test facility 2 (VTF2) at the High-Power Electric Propulsion Laboratory at the Georgia Institute of Technology. VTF2 is a cryopumped facility 9.2 m long and 4.9 m in diameter. It is brought to high vacuum with 10 CVI TMI reentrant cryopumps with a combined pumping speed of 350 000 l/s on xenon and a base pressure of 5×10^{-9} Torr. Pressure is measured with Varian 571 and UHV-24 ionization gauges mounted on opposite side of the vacuum chamber. The operating pressure, corrected for krypton, is maintained between 5.26×10^{-6} and 6×10^{-6} Torr-Kr. High purity krypton (99.9995%) is fed to the thruster with MKS 1179A mass flow controllers.

Plasma potential measurements inside the EEHET discharge channel are taken with a miniature floating emissive probe mounted on a high-speed axial reciprocating probe (HARP) system. The HARP is a computer controlled linear actuator that moves at 2 m/s to provide a residence time at the target location of ~130 ms. The emissive probe used in the measurements is constructed from 0.13 mm diameter thoriated tungsten filament to create a 1.3 mm diameter loop. The filament is housed in a 1.5 mm double bore alumina tube. The small size of the probe allows for interrogation of the plasma closer to the channel wall. To correct for the electron temperature mismatch between the emitted electrons and the plasma electrons, the measurement plasma potential is corrected by a factor of $0.6 \, T_e$ according to[5,13]

$$V_p = V_{p,raw} + 0.6 T_e. \tag{2}$$

Here, V_p is the calculated plasma potential in volts, $V_{p,raw}$ is the raw measured potential in volts, and T_e is the local electron temperature in eV. The electron temperature can be calculated from the floating potential by

$$V_p - V_f = -\frac{k_B T_e}{e} \ln\left(0.605 \sqrt{\frac{2\pi m_e}{m_i}}\right), \tag{3}$$

where V_f is the floating potential, k_B is the Boltzmann constant, e is the electron charge, and m_e and m_i are the electron and ion masses, respectively.

The channel plasma potential is mapped for an area 26 mm wide by 50 mm long covering the region of peak radial magnetic field and extending to within ~6 mm of the anode surface. Fig. 4 shows the area mapped with the probe and the locations of the measurements. The axial (z-axis) measurements are spaced 5 mm apart. The radial measurements are staggered (4, 4, 2, 2, and 1 mm steps on either side of centerline) in order to provide better resolution near the channel surfaces. Prior to data collection, the emissive probe heating current versus measured potential both inside and outside of the channel is plotted to ensure sufficient emission. Centerline potential measurements are also taken for multiple channel lengths downstream of the thruster exit. Fig. 5 shows the probe position and potential for a sample measurement. The oscillation in the thruster discharge current for the same time frame is shown in Fig. 6. The act of inserting the probe into the discharge channel causes a slight increase in the current oscillations, up to a 0.2 A spike in discharge current; for the ~200 ms, the probe spends inside the channel. This current spike is more evident closer to the anode and does not appear to affect the electrode current. Two sequential measurements at each location are averaged to reduce error. Uncertainty in the potential measurement is predominantly due to heating voltage causing a bias in the measured plasma potential. The heating voltage is a maximum of 5 V, thus providing an uncertainty of ± 5 V.
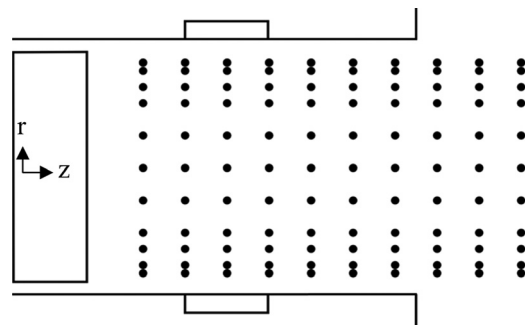

FIG. 4. Area and points mapped with the miniature emissive probe. Points are spaced 5 mm axially, and staggered in steps of 4, 4, 2, 2, and 1 mm radially from centerline.
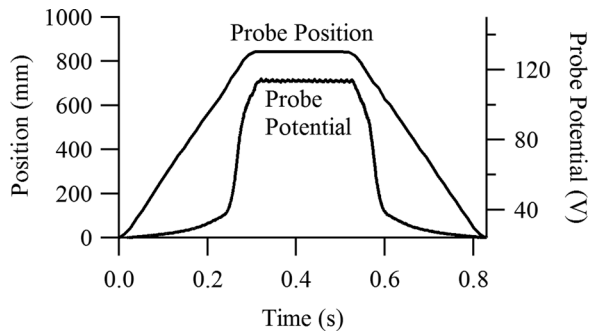
FIG. 5. Example of HARP position and measured probe potential. The potential is nearly flat for the short time and it is at the target location, and has a very steep rise and fall when the probe enters and leaves the discharge channel.
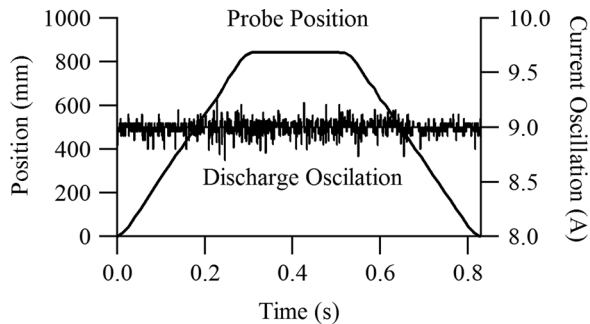

FIG. 6. Example HARP probe position and discharge current oscillations. The insertion of the probe causes small increase in discharge oscillation as measured at the discharge power supply line.

IV. RESULTS

A. Potential maps

The thruster was tested on krypton propellant at 150 V discharge and 9 ± 0.1 A. The thruster was run in constant current mode by varying the anode mass flow to maintain 9 A discharge current. The cathode flow rate is kept constant at 1 mg/s for all tests. The magnetic field is also kept constant for all tests to reduce variables, thus the magnets are not optimized for each operating point. In order to better understand the effect of the electrodes on the plasma potential, five separate electrode conditions are tested for each discharge setting. The graphite electrodes are tested at floating, 0, 10, and 30 V_e, where the subscript denotes volts electrode. In the floating condition, the electrodes are electrically isolated from any power supply and allowed to float in the plasma. In the 0 V_e condition, the electrodes are connected but no voltage is added to them. This biases the electrodes to the anode potential due to the electrical connections as shown in Fig. 2. In the 10 and 30 V_e conditions, 10 or 30 additional volts above anode potential are placed on the electrodes via their power supplies. In addition to the four electrode conditions, a fifth condition is tested where the graphite electrodes are replaced with BN rings of the same material as the rest of the channel. This condition approximates the standard HET channel and also gives insight into the effects of graphite presence on the plasma.

Fig. 7 shows the potential contour map for the BN and floating cases. The two maps show very similar field strengths and shapes. The cathode to ground voltage averaged −20 V,
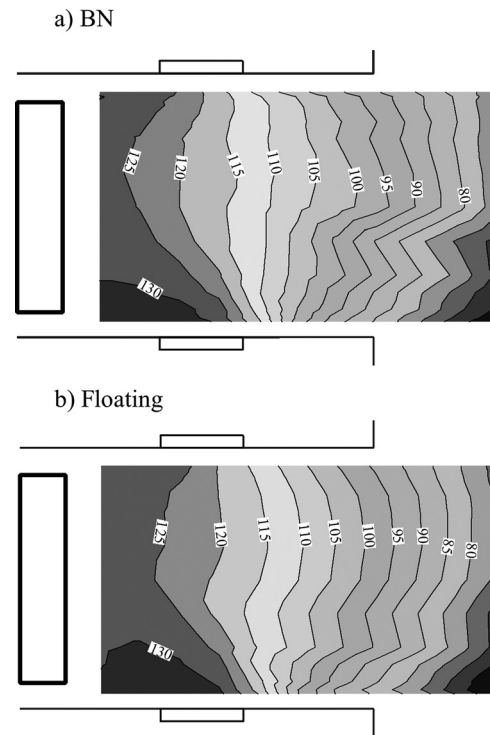

FIG. 7. Internal plasma potential contours for (a) BN and (b) floating cases.

thus the plasma potential is expected to be below 130 V for the BN and floating 150 V discharge. The floating case has a slight downstream shift of the potential contours. The similarity of the two maps indicates the presence of graphite does not have a significant impact on the plasma behavior. This is keeping in line with results obtained by Raitses et al.[14] He noted that graphite only affects the electron temperature and other plasma properties when the thruster was above 400 V. In addition, the placement of the graphite electrodes in the EEHET upstream of the magnetic field peak ensures that they are not exposed to high electron temperatures. This makes the differences in secondary electron emission between graphite and BN less important.

The floating condition exhibits largely radial contours. The contours also approximate the static magnetic field relatively well. The 130 V contour encloses a pocket region that is located at the cusp fields on the inner channel wall. On the opposite wall, however, no such closed contour exists. This may be due to the different surface area of the two electrodes. The outer electrode has more area due to the larger circumference and thus has a smaller local electric field. The downstream contours diverge from the magnetic field somewhat, but that is to be expected as the correlation between field lines and thermalized potential is not perfect and electron temperatures are high near the channel exit.[12]

Fig. 8 shows the potential maps for the other three electrode conditions, 0, 10, and 30 V_e. The anode voltage is maintained at 150 V, and the cathode to ground voltage is −19.8, −20, and −20.2 V, respectively. With biased electrodes, there are two main changes to the potential contours. The first is a division of the high potential regions at the upstream end of the channel near the electrodes. It can be seen clearly at 30 V_e, and somewhat at 0 and 10 V_e, that the
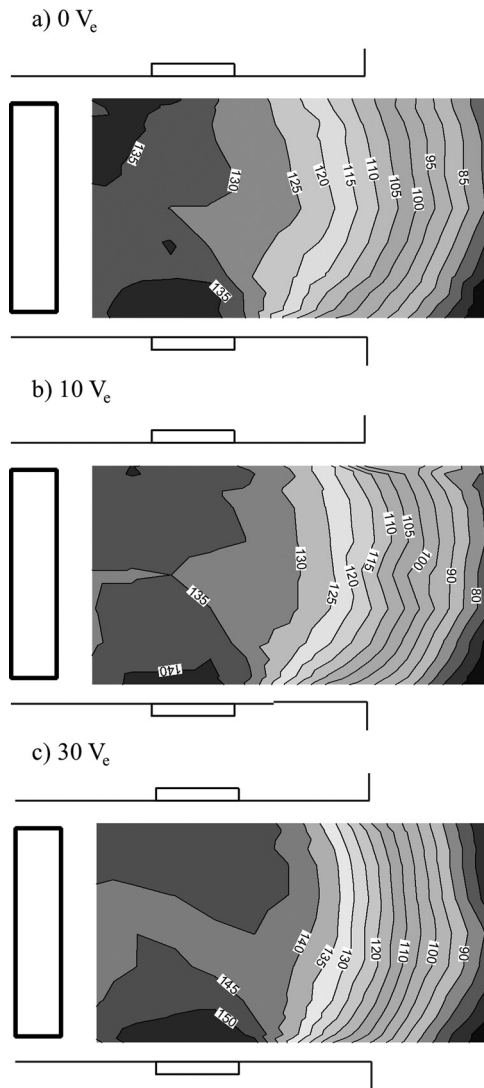
a) 0 V$_e$

b) 10 V$_e$

c) 30 V$_e$

FIG. 8. Internal potential contour maps for (a) 0 V$_e$, (b) 10 V$_e$, and (c) 30 V$_e$. The combination of biased electrodes and cusp-shaped fields cause pockets of high potential to occur.

high potential region near the anode and electrodes splits into two separate areas with a lower potential area between. To first order, these pockets of high potential conform to the cusp-shaped magnetic field regions as shown in Fig. 9. This
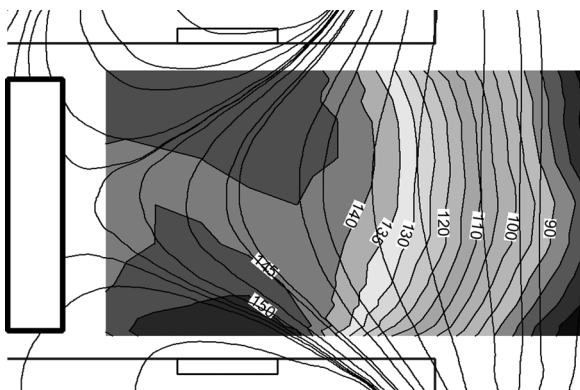

FIG. 9. 30 V$_e$ contour overlaid with static magnetic field. The pockets near the electrodes conform to the cusp fields.
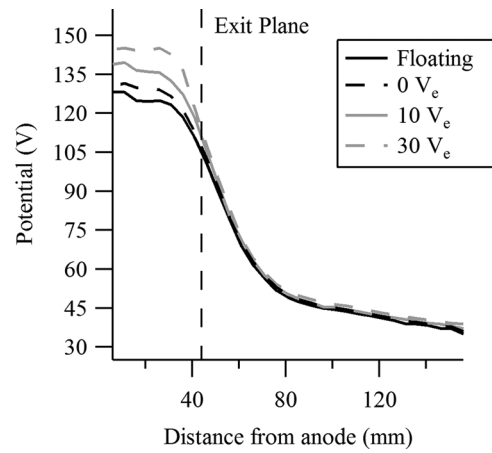

FIG. 10. Centerline potential profile for conditions tested.

pocketing of the potential will generate electric fields in the back of the channel pointed toward channel centerline.

The second main change that can be seen in the potential measurements is an increase in the potential range. When the electrode voltage is increased, the potential contours experience a similar increase in maximum potential. The minimum potential in the measurement region is relatively constant around 80 V. The far-field plasma potential, measured with a floating emissive probe at a 1 m distance from the channel exit, is also relatively stable, rising from 17.5 to 18.8 V with increased electrode voltage.[15] However, the maximum potential increases from 130 to 150 V with increased electrode voltage. The large increase in maximum potential with a small increase in downstream minimum potential results in a steeper potential profile. Fig. 10 shows the centerline

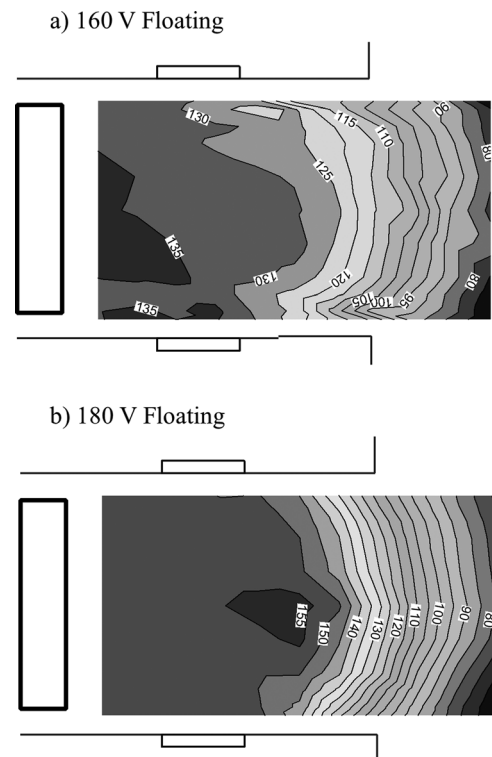a) 160 V Floating

b) 180 V Floating

FIG. 11. Internal plasma potential maps for (a) 160 V floating and (b) 180 V floating cases.

plasma potential profile for the four electrode cases out into the plume. As can be seen, the slope of the profile increases as the electrodes go from floating to 30 V_e. This can affect characteristics such as acceleration length which will be discussed in Sec. V.

Internal potential measurements were also taken at two additional floating conditions, 160 and 180 V discharge, to determine if the observed contour changes are due to the electrodes or the higher maximum voltage in the system. The thruster was tested at 160 V to compare to the 150 V, 10 V_e case, and 180 V for the 150 V, 30 V_e case. The two potential maps are shown in Fig. 11. The potential contours do not exhibit the contour pockets seen in the biased electrode cases. Thus, the contour pockets are a sole effect of the electrodes.

V. DISCUSSION

The two major effects of the electrodes are the creation of pocket contours, and a compression of the acceleration zone. From the BN and floating potential contours, there is a small pocket that exists near the inner electrode. However, its size and thus effect are small. The cusp magnetic fields may not be magnetizing electrons well at this condition. With the electrodes connected and biased, the cusp magnetic field seems to be able to magnetize electrons better and generates larger potential pockets. This is likely due to an expansion of the near-wall sheath that extends the electric field caused by the biased electrodes further into the bulk plasma. Previous research has shown that a magnetic field parallel or oblique to a surface can increase the thickness of the near-wall plasma sheath.[16–18] By extending the sheath, the electric field is able to affect a larger portion of the channel plasma thus creating larger potential pockets.

A related effect of the electrode use is a shift of the discharge current from the main anode to the electrodes. The original theory behind the cusp magnetic fields was to reduce electron current to the electrodes, reducing their power draw. However, that may not be actually true. At 10 V_e, the current to the electrodes is small, 0.59 A; thus, they can be assume to have little participation in the ion/electron current. However, at 30 V_e, the electrodes draw a substantial amount of current, 7.96 A. The overall discharge voltage is maintained at 9 A with the discharge power supply, due to the electrical connection of the electrodes and anode (the two share currents). Thus, 8 A on the electrodes means the anode only sees 1 A of current. This indicates the electrodes become the dominant positive terminal at 30 V_e. At this condition, the electrodes now dictate the plasma behavior similar to a higher voltage anode. Table I shows the operating conditions for the thruster at 150 V, including the plume properties of divergence angle, ion energy, and beam current. The beam current and plume divergence angle are determined from Faraday probe measurements according to the technique developed by Brown and Gallimore.[19,20] The uncertainty in the plume angle and beam current are ±5%. The ion energy systematic error is ±5.3 V.

The second major effect of the changing potential contours is an increase in the potential profile slope and a compression of the acceleration zone. The acceleration zone is an axial length where the majority of the potential drop and thus ion acceleration occurs. The electric field within this region is high. Fig. 12 shows the electric field for the electrode centerline profiles. The electric field is obtained simply as the axial derivative of the potential. The electric field for the 10 and 30 V_e cases is larger due to the increased potential drop.

The acceleration zone can be defined from the plasma potential as the region between 90% and 10% of the potential drop. The electric field can also be used to define the acceleration zone as the region between 0.15 E_{max}. Both of these methods have been used before with success.[5,21] Table II shows the results of these two methods for the four electrode cases. Shown are the start, end, and overall length of the acceleration zone. The potential method consistently calculates a start and end point further downstream than the electric field method. The length has larger changes with the potential method. One reason the potential method generates a longer acceleration zone is the lack of clarity when defining the final minimum plasma potential. As Fig. 10 shows, the plasma potential still decreases in the plume. The change is much smaller than near the exit plane, but it makes the calculations somewhat subjective. The electric field method also has faults. A larger electric field will increase the 0.15 E_{max} value, thus changing the determination for zone location. The potential field method is the more reliable method as it is only affected by the axial measurement range, which

TABLE I. Voltage and current conditions for floating, 10 and 30 V_e potential maps at 150 V discharge.

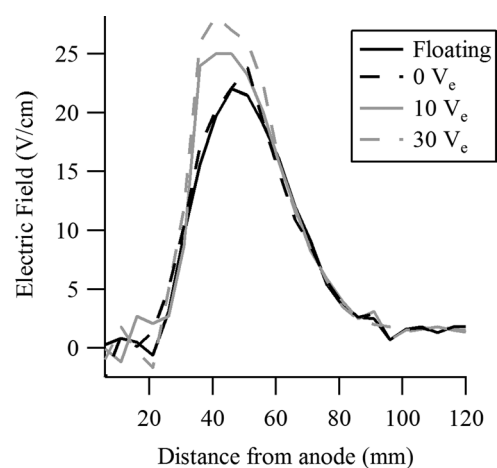|	Floating	10 V_e	30 V_e
Anode current (A)	9	8.41	1.08
Electrode current (A)	0	0.55	7.96
Discharge voltage (V)	150.05	150.65	150.4
Cathode to ground (V)	−19.3	−18.95	−20.4
Plume half angle (deg)	73.6	72.8	71.1
Most probable ion energy (V)	90.2	91.6	99.3
Ion beam current (A)	5.71	5.88	5.98
Thrust (mN)	58.87	63.4	66.4

FIG. 12. Centerline electric field.

TABLE II. Acceleration zone defined by plasma potential and electric field. All lengths have systematic error of ± 3 mm.

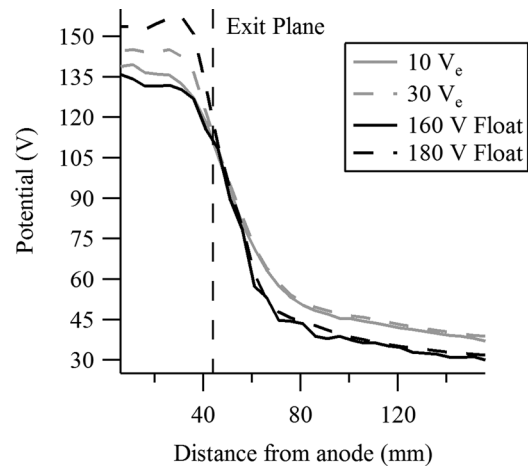|	Floating	0 V_e	10 V_e	30 V_e
Potential				
Start (mm)	35	36	37	37
End (mm)	108	104	91	87
Length (mm)	**73**	**68**	**54**	**50**
Electric field				
Start (mm)	26	24	27	25
End (mm)	88	83	85	82
Length (mm)	**62**	**59**	**58**	**57**

FIG. 13. Centerline plasma potential measurements for 160 and 180 V floating compared to the 10 and 30 V_e data.
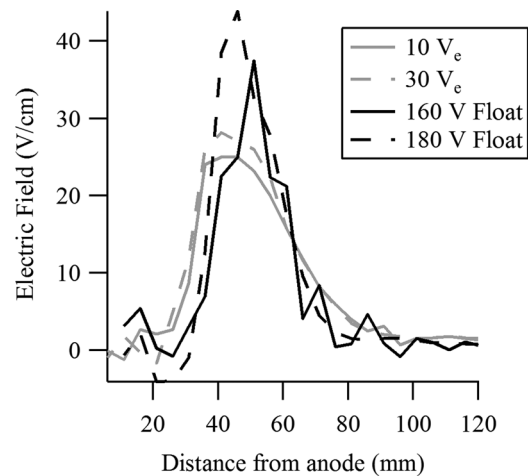

FIG. 14. Electric field for 160 and 180 V floating compared to the 10 and 30 V_e data.

TABLE III. Acceleration zone values for the 160 and 180 V floating cases.

	150 V 10 V_e	150 V 30 V_e	160 V Float	180 V Float
Potential				
Start (mm)	37	37	36	38
End (mm)	91	87	80	79
Length (mm)	**54**	**50**	**44**	**41**
Electric field				
Start (mm)	27	25	34	34
End (mm)	85	82	79	82
Length (mm)	**58**	**57**	**45**	**48**

if consistent for all operating conditions allows fairly clear comparisons to be made.

With either method, the acceleration zone decreases in length with the electrodes. This is a combination of downstream movements of the zone start and upstream movements of the zone end, thus a compression of the region. The two methods disagree on the magnitude of compression, with the potential method having a rather large compression of 23 mm from floating to 30 V_e. Nonetheless, the compression is a definite effect. Shortening of the acceleration zone can affect the ion trajectories and losses. The electric fields near the thruster exit have some degree of divergence which will cause ions to have increase radial velocities. This in turn increases plume divergence angle. With a shorter acceleration zone, ions spend less time on the diverging fields and thus have less plume divergence. Plume divergence angle was measured using a Faraday probe attached to a 1 m probe arm. The probe was swept from 0° to 180° through the thruster plume. The integrate current density from the Faraday probe allows determination of the plume divergence angle following the procedures outlined by Brown and Gallimore.[19,20] The plume divergence angle for the conditions shown here is given in Table I.

In addition to decreased divergence, a shorter acceleration zone decreases the probability of ion collisions that may result in neutralization or charge exchange. Ions neutralized by collisions with other particles during acceleration will exit the thruster with less than full velocity, thus decreasing thrust. Charge exchange collisions occur when a high energy ion collides with a low energy neutral. The two particles exchange energy but retain their charge. The result is a slow ion generating less thrust, and a fast neutral producing no thrust.

A similar analysis of the acceleration zone is done for the 160 and 180 V floating cases. The results are shown in Figs. 13 and 14 and summarized in Table III. Also shown for direct comparison are the 10 and 30 V_e data. The two methods for calculating the acceleration zone do not agree on the length consistently. However, both methods indicate the two floating cases have smaller acceleration zones than the electrode cases by ~8 mm. This goes further to prove that the electrodes are causing different plasma behaviors than a standard increase in voltage.

The changing in-channel potential contours create a focusing effect by virtue of the domed potential regions. The resultant electric field is normal to the potential lines and focus ions toward the center of the channel, reducing ion wall neutralization losses. This in turn could cause the increased ion beam current, which directly contributes to the increase thrust and decreased plume divergence angle. At 30 V_e, there is the additional factor of increased ion energy due to the current shifting from anode to electrodes. In this case, some portion of the observed thrust improvements is caused by the higher energy ions resulting in higher exit velocity. The decrease in the acceleration region also contributes to

the decreased plume divergence angle. As the acceleration region is compressed inward, the apparent channel exit angle for ions decreases. Thus, ions which may exit the thruster at large angles in the floating condition may collide with the channel walls in the 30 V_e condition, decreasing the measured plume divergence. However, this ion loss is likely a small number as the overall ion beam current and, thus, ion number density, increase with electrode potential.

A. Sheath behavior with cusp-magnetic fields

An area of interest of this work with in-channel electrodes and their shielding cusp fields is the interaction of the magnetic field with the near-wall plasma sheath. The plasma sheath is a thin region of plasma that surrounds any surface exposed to the plasma whether it be insulating or conducting. For an insulating surface, the sheath exists due to the different velocities of electrons and ions. As the insulating surface will float to a potential less than the plasma potential, an electron repelling sheath, or potential drop, forms to maintain a monotonic sheath potential drop from plasma potential to wall potential.

For a conducting surface, such as the biased electrode configurations, the sheath around the electrode becomes controlled by the need to balance the electron current into the electrodes. For the case here, a positively biased electrode, the sheath formed is typically an electron repelling sheath. The sheath size is controlled by the balance between the electron flux to the conducting surface and the current draw necessary to maintain the discharge. In most cases, the electron flux is higher than necessary for the discharge, thus an electron repelling sheath develops to reduce the flux. A larger disparity requires a thicker sheath. It is also possible to have an electron attracting sheath if the thermal flux is insufficient to maintain the discharge current. This situation is present in cases of electrodes with surface areas too small for sufficient flux.[22,23] Between the two sheath types is a no-sheath regime where the flux equals the electron current draw by the discharge.

Another method to control the electron flux to electrodes is with magnetic fields, specifically fields parallel or at small angles to the electrodes. The cusp fields that surround the wall electrodes in this work are one such example. The presence of strong magnetic fields can magnetize electrons, reducing their mobility, and fluxes toward the electrode. This in effect performs the function of an electron repelling sheath, and can reduce or remove the sheath thickness. Magnetization of electrons occurs if the electron Hall parameter, Ω_e, is much larger than unity,

$$\Omega_e^2 = \frac{\omega_e^2}{v_e^2} \gg 1. \tag{4}$$

Here, ω_e is the electron gyro frequency, and v_e is the electron collision frequency. The gyro frequency and collision frequency are

$$\omega_e = \frac{qB}{m}, \tag{5}$$

$$v_e = 2.91 \times 10^{-6} n_e \Lambda T_e^{-3/2}, \tag{6}$$

where q is the particle charge, B is the magnetic field in Tesla, m is the electron mass, n_e is the electron number density in cm^{-3}, Λ is the Coulomb logarithm taken as 10 for this first order analysis, and T_e is the electron temperature in eV. The magnet field in the cusps 3 mm from the surface, approximately where the closes probe point is taken, is around 250 G. The channel electron density can be calculated to first order from[24]

$$n_e = \frac{I_b}{ev_b A_c} = \frac{\eta_b I_d}{eA_c \sqrt{\frac{2\eta_b eV_d}{M}}}. \tag{7}$$

Here, I_b is the measured ion beam current, e is the electron charge, v_b is the beam velocity, A_c is the channel area, η_b is the beam efficiency with is equal to beam current divided by discharge current (I_b/I_d), and M is the ion mass. This calculation yields an electron density between 1.27 and 1.3×10^{17} m^{-3}. The uncertainty in the ion beam current causes a 4% error in the electron density.

Electron temperature is calculated from the difference between the plasma and floating potential measured by the emissive probe from

$$V_p - V_f = -\frac{k_B T_e}{e} ln\left(0.605\sqrt{\frac{2\pi m}{M}}\right). \tag{8}$$

Here, V_p is the plasma potential, V_f is the floating potential, and k_B is the Boltzmann constant. This equation is based on the assumption of Maxwellian electrons with temperatures much higher than the ions, which is generally true in HETs. The resulting electron temperature map for the 30 V_e case is shown in Fig. 15. The average electron temperature near the electrodes is 10 eV. This resulting electron Hall parameter squared is 22.9, which means the electrons are magnetized. The electron temperatures are similar for the other electron cases tested, thus electron magnetization would occur for all electrode cases tested, BN to 30 V_e. This leads to the conclusion that the sheath should be strongly affected by the cusp magnetic field.
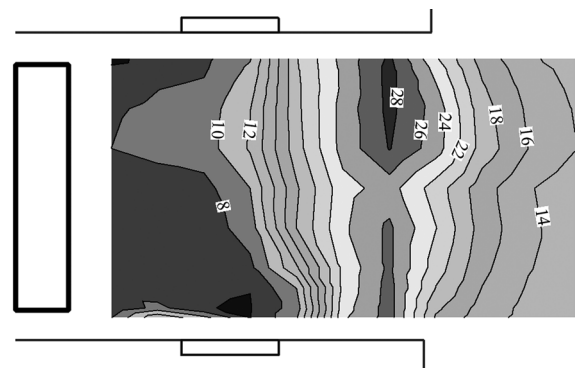

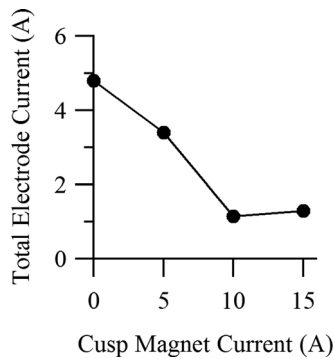FIG. 15. Electron temperature map for 150 V, 30 V_e case.

FIG. 16. Total electrode current (for both electrodes) as a function of the cusp magnet current. The thruster was operated at 175 V, 9 A discharge with 10 V_e electrodes. Both cusp magnets had the same current. For reference, the cusp magnets were at 15 A for all the in-channel measurements.

The magnetization of the electron causes a reduction of electron flux to the electrodes. This can be seen from a plot of cusp magnet current versus the electrode current as shown in Fig. 16. The thruster was run at 175 V, 9 A at constant mass flow. The inner and outer cusp magnet currents were varied at the same time to maintain symmetry. For the in-channel measurements, the cusp magnets were held constant at 15 A. This behavior suggests that the sheath shrinks in size as the electron flux to the electrodes is reduced by the magnetic fields. It was also observed that an increase in one cusp magnet, the inner or outer, causes a drop in the associated electrode current and increases in the other. For example, an increase in the inner cusp magnet strength decreases the inner electrode current but increases the outer electrode current. However, the total electrode current remained nominally constant. The mass flow and discharge voltage are held constant; thus, the shifting of currents is due to changing magnetization of electrons around one electrode, causing the other electrode to draw more current to maintain the discharge. This would mean the inner and outer electrode sheaths grow and shrink in a dependant fashion, which is logical given that they are both tied into the same electric circuit. All in all, the electron behavior indicates that the cusp magnetic fields are having a significant effect on the electron flux and sheath properties. Further investigation is needed to better quantify the interactions.

VI. CONCLUSION

This paper details internal plasma potential measurements of a HET using embedded graphite electrodes. The presence of graphite in the BN channel does not significantly change the potential contours, which agrees with work done by other researchers. With biased electrodes, there are changes in the potential contours near the electrodes. Closed pocket contours are observed with electrodes biased 10 and 30 V above anode potential. The electrodes also cause a compression of the acceleration zone similar to, but smaller in magnitude, that seen with the same increase in discharge voltage. The potential contour pockets are also not observed in higher discharge voltage floating cases. The presence of the pockets is attributed to the dual effect of the cusp-shaped magnetic fields and the electrode bias. The near-wall plasma sheath around the electrodes appears to be significantly affected by the cusp magnetic fields. The electrode current is reduced with stronger magnet field, and even shifts between the two electrodes when the current on one of the magnets is increased. Further investigation of the near-wall sheath and/or computational analysis is necessary to better understand the effects of the cusp magnetic fields and electrodes on the sheath and electron behavior.

[1]K. G. Xu and M. L. R. Walker, presented at the 47th AIAA Joint Propulsion Conference, San Diego, CA, 2011.

[2]J. B. McVey, E. J. Britt, S. F. Engelman, F. S. Gulczinski, E. J. Beiting, and J. E. Pollard, presented at the 39th Joint Propulsion Conference, Huntsville, AL, 2003.

[3]R. R. Hofer, Ph.D. thesis, University of Michigan, Ann Arbor, 2004.

[4]J. M. Haas, Ph.D. thesis, University of Michigan, Ann Arbor, 2001.

[5]B. M. Reid, Ph.D. thesis, University of Michigan, Ann Arbor, 2009.

[6]V. M. Gavryshin, V. Kim, V. Kozlov, and N. A. Maslennikov, in *24th International Electric Propulsion Conference*, Moscow, Russia (Electric Rocket Propulsion Society, 1995), IEPC Paper No. 95–38.

[7]A. W. Kieckhafer, Ph.D. thesis, Michigan Technological University, Houghton, 2007.

[8]Y. Raitses, M. Keidar, D. Staack, and N. J. Fisch, J. Appl. Phys. **92**(9), 4906 (2002).

[9]Y. Raitses, L. A. Dorf, A. A. Litvak, and N. J. Fisch, J. Appl. Phys. **88**(3), 1263 (2000).

[10]I. G. Mikellides, I. Katz, R. R. Hofer, and D. M. Goebel, presented at the 46th AIAA Joint Propulsion Conference, Nashville, TN, 2010.

[11]A. I. Morozov, Yu. V. Esipchuk, G. N. Tilinin, A. V. Trofimov, Yu. A. Sharov, and G. Ya. Shchepkin, Sov. Phys. J. **17**(1), 38 (1972).

[12]V. V. Zhurin, H. R. Kaufman, and R. S. Robinson, Plasma Sources Sci. Technol. **8**(1), R1 (1999).

[13]J. A. Linnell and A. D. Gallimore, presented at the 41th AIAA Joint Propulsion Conference, Tucson, AZ, 2005.

[14]Y. Raitses, I. D. Kaganovich, A. Khrabrov, D. Sydorenko, N. J. Fisch, and A. Smolyakov, IEEE Trans. Plasma Sci. **39**(4), 995 (2011).

[15]K. G. Xu, Ph.D. thesis, Georgia Institute of Technology, Atlanta, 2012.

[16]A. Anders, Surf. Coat. Technol. **136**, 85 (2001).

[17]M. Keidar and I. I. Beilis, Appl. Phys. Lett. **73**(3), 306 (1998).

[18]I. I. Beilis and M. Keidar, Phys. Plasmas **5**(5), 1545 (1998).

[19]D. L. Brown and A. Gallimore, Rev. Sci. Instrum. **81**, 063504 (2010).

[20]D. L. Brown and A. D. Gallimore, J. Propul. Power **27**(3), 573 (2011).

[21]J. A. Linnell, Ph.D. thesis, University of Michigan, Ann Arbor, 2007.

[22]L. Dorf, Y. Raitses, and N. J. Fisch, J. Appl. Phys. **97**, 103309 (2005).

[23]A. Anders and S. Anders, Plasma Sources Sci. Technol. **4**, 571 (1995).

[24]D. M. Goebel and I. Katz, *Fundamentals of Electric Propulsion: Ion and Hall Thrusters* (Jet Propulsion Laboratory, Pasadena, 2008).